International Journal of Thermal Sciences 148 (2020) 106145

Contents lists available at ScienceDirect

International Journal of Thermal Sciences

journal homepage: http://www.elsevier.com/locate/ijts

Performance analysis and shape optimization of a water-cooled impingement micro-channel heat sink including manifolds

Yaser Hadad [a], Srikanth Rangararajan [a,*], Kourosh Nemati [b], Bharath Ramakrishnann [a], Reza Pejman [a], Paul R. Chiarot [a], Bahgat Sammakia [a]

[a] Department of Mechanical Engineering, State University of New York at Binghamton, Binghamton, NY, USA
[b] Future Facilities Ltd, New York, NY, USA

ABSTRACT

Impingement micro-channel heat sinks are in general preferred over parallel flow micro-channel heat sinks owing to the reduced pressure drop. Splitting the flow in two branches cuts the flow rate and path in half, which leads to lower pressure drop through the channels in impingement heat sinks compared to a parallel flow heat sink. A numerical model was developed to predict the heat sink performance. Because of the significant effect that inlet and outlet manifolds (distributor and collector) have on the heat sink hydraulic and thermal performance, the numerical model includes them. The model was validated both for hydraulic and thermal performance using experimental data. The model was used for shape optimization of the heat sink in constant chip power, coolant inlet temperature and flow rate as well distributor and collector geometry. A parametric study was performed to estimate the effect of the geometric design parameters on the hydraulic and thermal resistances as the response parameters. The chip-base interface temperature profile was very different from typical parallel heat sinks. The coefficient of performance as a measure of the heat sink overall performance (hydraulic and thermal) was measured experimentally. Furthermore, the sensitivity of the heat sink coefficient of performance to chip power, coolant inlet temperature and flow rate was estimated using a regression model fitted on the obtained experimental result.

1. Introduction

Owing to the ever-shrinking size of the electronic equipment, it necessitates higher circuit integration per unit area, which in turn contributes to a rapid increase of heat generation. Thus, the effective removal of heat dissipations and maintaining the chip at a safe operating temperature has played an important role in insuring a reliable operation of electronic components. In practice, the most popular cooling method takes the form of air-cooling. However, air-cooling suffers from low heat transfer performance and noise problems. To address this difficult situation, liquid cooled heat sinks with various designs (geometries) are considered. With their high specific heat capacity, thermal conductivity, and density, liquids are able to receive, store, and carry higher amount of energy compared to air. Liquid's incompressibility and very low specific volume requires smaller amounts of mechanical work for their circulation. Compact and high-performance forced liquid cooling of planar integrated circuits has been investigated numerously in literature. The convective heat-transfer coefficient between the substrate and the coolant was found to be the primary figure of merit to achieve low thermal resistance. For laminar flow in confined parallel channels, convection coefficient scales inversely with channel width, making flow through the microscopic channels desirable. Therefore, liquid (water)-cooled heat sinks have drawn recent attention to their application, design, and optimization. The state of the art work in achieving high heat flux cooling of the order of 790 W/cm^2 by forced liquid cooling through parallel channels was achieved by Tuckerman and Pease [1]. In forced convection liquid cooling various parameters like the channel geometry, fin geometry, flow parameters (temperature, flow rate) have seen to play an important role in achieving high performance.

The influence of coolant flow rate on the hydraulic and thermal performance of water-cooled rectangular parallel micro-channel heat sinks was studied in Refs. [2–5]. The results show that dies with heat flux between *100-200* W/cm^2 can be cooled with flow rate up to $1 lit/min$ of water with acceptable values of pressure drop. Using the theory of extended surfaces and laminar boundary layer solution, analytical models were developed to predict the hydraulic performance (pressure drop) and the thermal performance (channel Nusselt number and heat sink thermal resistance) in rectangular parallel micro-channel heat sinks [6–8]. Parametric studies were done to investigate the effect of geometric parameters such as fin thickness, space, and height on the thermo-hydraulic characteristics of liquid-cooled heat sinks with rectangular parallel micro/mini-channels [9–11]. Ermagan and Rafee [12] studied the effect of channels number and width on the thermal

* Corresponding author.
E-mail address: srangar@binghamton.edu (S. Rangararajan).

https://doi.org/10.1016/j.ijthermalsci.2019.106145
Received 6 March 2019; Received in revised form 15 August 2019; Accepted 14 October 2019

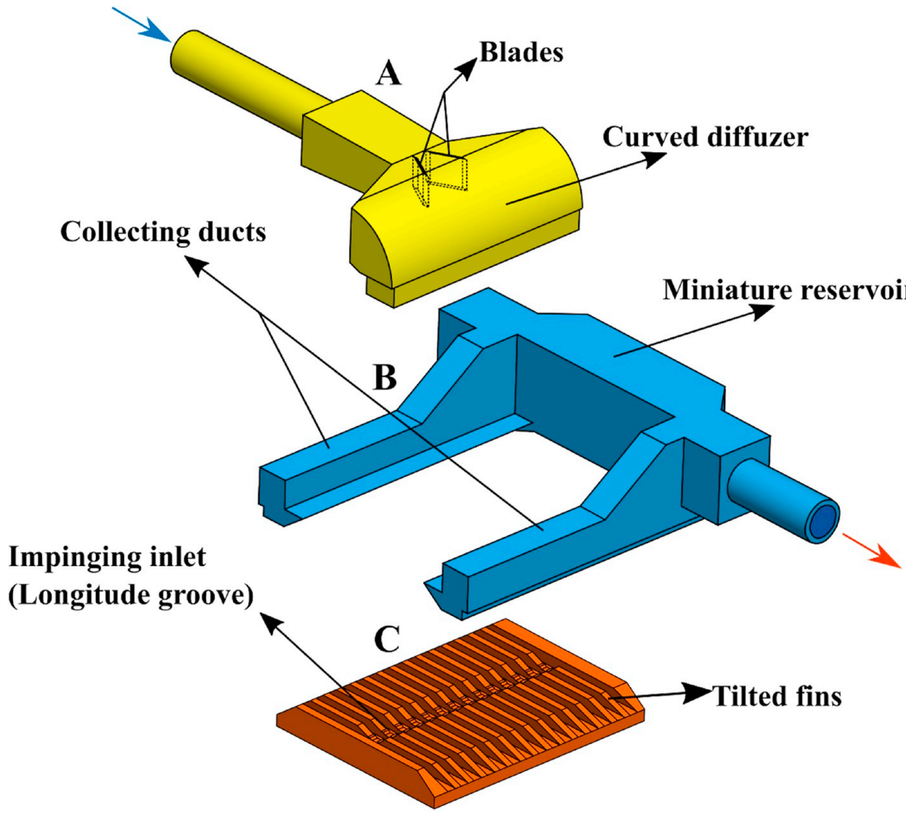

Fig. 1. A schematic exploded view of the predefined heat sink (A) distributor, (B) collector, and (C) micro-channel network.

resistance of a water-cooled rectangular parallel channel heat sink with three different wall hydrophobicities at constant pump power. Geometric optimization was done to obtain the optimal designs of liquid-cooled double-layer parallel micro-channel heat sinks with different flows direction at the top and bottom layers in Refs. [13,14]. In order to improve thermal performance, liquid-cooled parallel micro-channel heat sinks with different wall architectures such as triangular cavities and rectangular ribs [15], fan-shaped ribs [16–19], wavy/zigzag channels [20,21], as well as heat sinks with grooves and obstacles in the channels [22–27] were studied numerically and experimentally. Huang et al. [28] showed that the thermo-hydraulic performance of liquid-cooled parallel micro-channel heat sinks is improved by using slotted arrangements. They numerically studied the performance of rectangular parallel-slot, rectangular staggered-slot, and trapezoidal staggered-slot micro-channel heat sinks. The effect of porous substrates on the hydraulic and thermal performance of water-cooled rectangular parallel micro-channel heat sinks was investigated by Ghahremannezhad et al. [29,30]. Liquid-cooled parallel flow heat sinks containing micro-pin fins were studied to investigate the effect of geometrical parameters (fin diameter, cross section, porosity, and array) on pressure drop and thermal resistance [31,32].

If not for the extra height consumed for the operation, impingement cooling is preferred to parallel-flow cooling method owing to its reduced pressure drop. Impingement flow is an umbrella term for certain types of flow where flow direction changes typically by 90° by striking a solid surface [33]. For an impinement flow, hydraulic and thermal boundary layer shapes are thoroughly different from those of parallel flows that leads to different hydraulic and thermal behavior. Parallel water-cooled heat sinks have been studied and optimized for different dimensions (micro and/or mini channels) and under different hydraulic and thermal boundary conditions extensively. Water-cooled impingement heat sinks, however, are quite modern and have not studied extensively. Furthermore, water-cooled impingement heat sinks have drawn recent attention due to their higher thermo-hydraulic performance.

Heat transfer characteristics of impingemet flow of transformer oil and 3 M fluorinert liquid FC-72 in two-dimensional micro-channels were studied by Zhuang et al. [34]. They measured local heat transfer coefficient both at stagnation and parallel flow regions in the Reynolds number range of 70 – 170 and 911 – 4807 for oil and FC-72, respectively. The effects of coolant Prandtl number and velocity, and channel geometry on heat transfer performance were examined. Lelea [35,36] studied the hydraulic and thermal performance of water-cooled impingement micro-tube heat sinks with single and multiple inlets positioned tangentially on the tube axis. The effect of operational and geometric parameters on the heat transfer characteristics of liquid-cooled impingement pin-fin heat sinks were evaluated in Refs [37–39]. The heat transfer enhancement technique of nanofluids together with methods for increasing nano-particles Brownian motion (flow pulsation and magnetic field) in the base fluid flow was employed to increase the thermo-hydraulic performance of parallel micro-channel and liquid-cooled impingement pin-fin heat sinks [40–44]. The channel-network of a split microchannel (impingement) heat sink designed to work with warm water (as the coolant) was optimized to reduce hydraulic and thermal resistances [45].

By distributing the flow through the channels, manifolds do effect the hydraulic and thermal performance of the heat sinks. Manifolds with different designs and architecture, work for parallel channel heat sinks, have been studied and optimized to approach uniform flow distribution [46–52]. The assumption of uniform flow distribution has been applied to a large number of previous numerical studies and optimizations of liquid-cooled heat sinks [6,7,9–15,17–20,22,23,53–56]. However a question is how much uniform flow assumption is realistic for different (parallel and impingement) designs? In the present study, manifolds were solved together with channel network because of two reasons. First, it brings the simulation closer to reality. Second, for validating the model, it is much simpler to measure the pressure drop through the whole device (in comparison to measuring the pressure drop through the channels) and compare it with acquired numerical data.

Different DOE (design of experiments) methods in conjunction with different optimization algorithms has been using for optimizing the geometric and/or operational parameters of heat transfer devices. The RSM (response surface methodology) associated with SAO (sequential approximation optimization) algorithm were used to optimize the geometric parameters of a pin-fin heat sink [57] and a parallel-plain heat sink [58] for pressure drop and thermal resistance. Using RSM together with iterative JAYA algorithm Rao et al. [55] performed a dimensional optimization to minimize the pumping power and thermal resistance of a micro-channel heat sink. DOE orthogonal arrays and a grey-based FUZZY algorithm were used by Chou et al. [59] to optimize the hydraulic and thermal performance of a parallel-plain fin heat sink. RSM with FCCCD (face centered central composite design) was employed for multi-objective optimization of a honeycomb heat sink by Subasi et al. [60]. They calculate the optimal values of the heat sink geometric parameters and Reynolds number that offer the maximum Nusselt number and minimum friction factor. Wen et al. [61] optimized the configuration of a serrated fin in plate-fin heat exchanger using a GENETIC algorithm combined with Kriging response surface method. They calculated the optimal values of the geometric parameters, which maximize the Colburn factor and minimize the Fanning friction factor. Evolutionary algorithms were utilized for multi-objective optimization of an impingement pin-fin heat sink [62]. The optimal geometrical design was posed to minimize the junction temperature and the fan pumping power of the heat sink. Using RSM together with JAYA algorithm, Hadad et al. [63] optimized the thermo-hydraulic performance of a multi-die micro-channel heat sink. They compared the results of the weight optimization with the results calculated by the non-dominated sorting GENETIC algorithm. Comprehensive review studies on the design, optimization, and fabrication of liquid-cooled heat sinks with a wide variety of architectures and applications are available in Refs. [64,65].

In this study, a water-cooled impingement micro-channel heat sink was modelled and optimized numerically. The model includes distributor and collector that supply fluid to the heat sink. It is desirable to develop models including the distributor and collector since the experimentally measured pressure drop must include these components. The geometry of the distributor and collector in impingement heat sinks is more complicated than in parallel flow heat sinks due to the more flow directions (one inlet at the top and two outlets on the sides). The main challenge in modeling the whole heat sink geometry is generating a grid with acceptable mesh metrics in regions with an abrupt change in length scale. These regions are located near the exit of the distributor (channel network entrance) and the entrance of the collector (channel network exit). The experimental analysis of the hydraulic and thermal performance of current geometry (predefined design) is presented in Ref. [66]. To the best of our knowledge, the work presented in this manuscript becomes a precursive study on modeling and optimization of a water-cooled impingement micro-channel heat sink including its distributor and collector.

2. Predefined heat sink geometry and dimensions

The predefined heat sink geometry consists of three main parts: distributor, micro-channel network (including fins and channels), and collector. Fig. 1 shows a schematic exploded view of the whole heat sink. The distributor (Part A) consists of a short inlet pipe, a curved diffuser and a rectangular duct that connects the entrance pipe to the diffuser. The curved diffuser has a rectangular cross section and by changing the flow direction by 90° it supplies the coolant to the micro-channel network. Two blades placed in the diffuser entrance divide the flow into three paths and make the flow uniform at the exit. A schematic of the micro-channel network is showed in Fig. 1 (Part C) with an exaggeration in the fin thickness and channel width. The micro-channel network of the heat sink consists of almost 100 impingement micro-channels connected by a longitude groove with a nearly trapezoidal cross section that is called the impinging inlet (Fig. 1). The flow supplied to the impinging inlet by the curved diffuser is distributed to the micro-channels in two opposite directions. The impinging inlet directs the coolant flow exiting the diffuser to the micro-channels. By distributing the flow smoothly and gradually, a well-designed impinging inlet reduces the flow minor losses and maldistribution. As showed in Fig. 1, the fins are not vertical in the predefined heat sink design. Part B in Fig. 1 is a schematic of the collector. Two parallel ducts in the collector gather the flow existing the micro-channels and carry it to a miniature reservoir. Finally, a circular cross section duct directs the flow from the miniature reservoir to the exit. Fig. 2 is an image of the heat sink's main two parts. The micro-channel network is made of copper and includes the fins and the impinging inlet (Fig. 2 (A)). The heat sink cap is made of plastic and consists of the distributor and collector (Fig. 2 (B)).

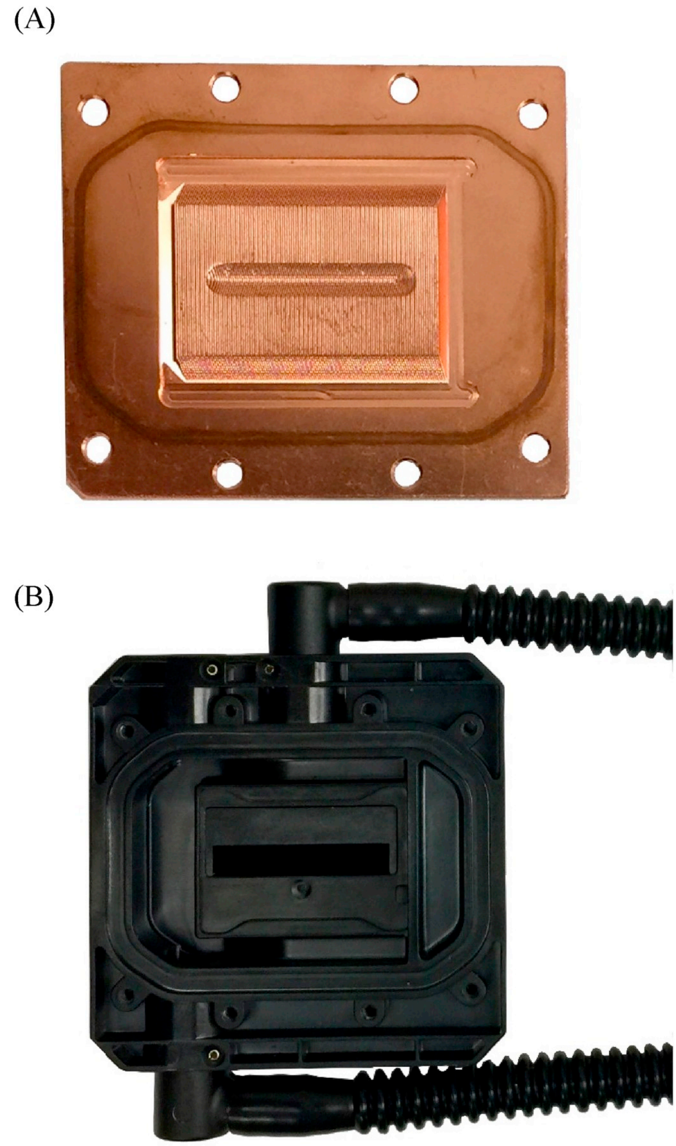

Fig. 2. Manufactured water-cooled impingement micro-channel heat sink. (A) Micro-channel network made of copper including fins, base and impinging inlet. (B) Heat sink cover including distributor and collector.

Obtaining micrographs of the heat sink micro-channels in order to measure its dimensions is difficult. To measure the fin thickness, space (channel width), height, and tilt angle accurately the micro-channel network was filled with epoxy and then cut down the middle. After polishing the cut surface, a stereo microscope was used to image the cross section (Fig. 3). The geometric parameters of the predefined design

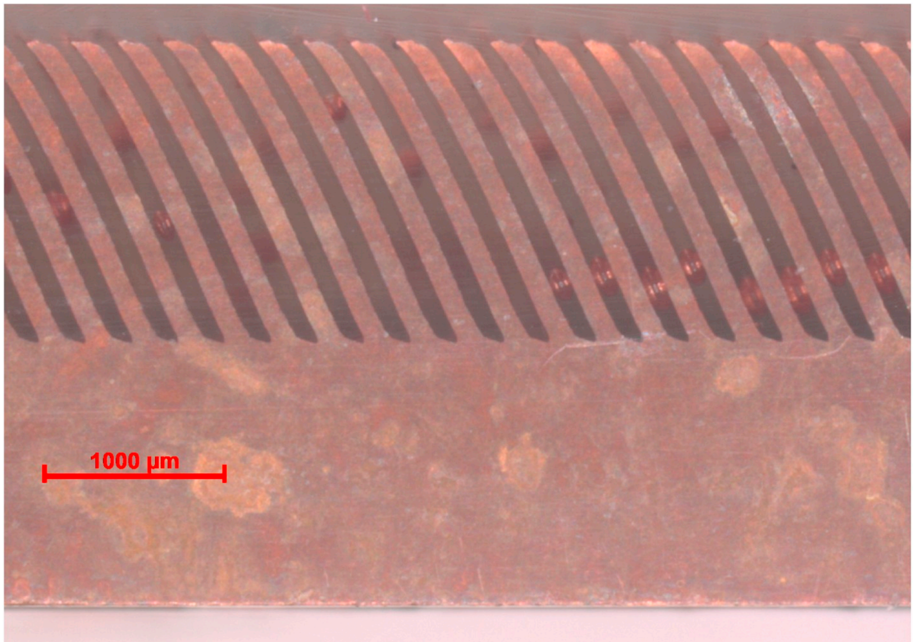

Fig. 3. A micrograph taken by a stereo microscope, showing channels and fins cross section and used for measuring base thickness, channel width, fin thickness, height, and tilt angle.

are showed on a schematic of a channel in Fig. 4. Table 1 presents the parameter definitions and their corresponding values.

3. Coolant and metal properties

The current problem is a conjugate (conduction-convection) heat transfer problem that involves both solid and liquid thermo-physical properties. The thermo-physical properties of pure copper at room temperature was applied to the micro-channel network of the heat sink. The coolant is a 15% propylene glycol aqueous solution at 300 K. Adding propylene glycol to water prevent the micro-channel network (metal part) from eroding. However, it increases the water viscosity and results in a pressure drop penalty. Comparing pure water viscosity with that of 15% propylene glycol aqueous solution we find 74% increase in viscosity. The thermo-physical properties of the solid phase and coolant are showed in Table 2 for reference.

4. Numerical analysis

4.1. Basic assumptions

A few basic assumptions are made in both the hydraulic and thermal characteristics of the model for simplification.

1. The flow is three dimensional, steady, laminar (low Reynolds number in channels ($Re_{Ch} < 100$) and distributor and collector (Re_{Di} & $Re_{Co} < 1000$)), and incompressible.
2. The effect of gravity is negligible.
3. Thermo-physical properties of the solid and liquid phase are constant.
4. Viscous heating and radiation heat transfer are neglected.
5. The whole module (electronic chip and heat sink) is insulated and there is no heat transfer to the ambient via free convection or radiation.

4.2. Governing equations

In order to determine the flow field inside the channels, distributor, and collector, the equations of motion and continuity were solved. The energy equation was also solved for the flow inside the channels and for the solid portion (i.e. fins, base) of the micro-channel network in order to capture temperature field. The governing equations are expressed as the

Conservation of mass (continuity):

$$\nabla.\vec{V} = 0 \tag{1}$$

Equations of motion:

$$\rho_f\,(\vec{V}.\nabla)\vec{V} = -\nabla P + \mu_f \nabla^2 \vec{V}, \tag{2}$$

Energy equation for liquid phase:

$$\rho_f c_{p,f}\,(\vec{V}.\nabla)T_f = k_f \nabla^2 T_f, \tag{3}$$

Laplace equation of conduction for channel network:

$$\nabla^2 T_s = 0. \tag{4}$$

4.3. Computational domain and boundary conditions

The space surrounded by the distributor and collector surfaces and the entire micro-channel (copper) network of the heat sink constitute the computational domain. The distributor and collector surrounding surfaces all are considered as no-slip adiabatic rigid walls. Fig. 5 shows the computational domain associated with the hydraulic and thermal boundary conditions. The coolant enters the distributor with identified flow rate/velocity ($Q = 0.35\ lit/min = 5.83\ cm^3/s$) and inlet temperature ($T_{In} = 27^{\circ}C \approx 300K$). An electronic chip with a power of 150W and surface area of 5.588 cm^2 provides a constant heat flux of almost 27 W/cm^2 on the bottom of the micro-channel network. Outflow boundary condition was applied to the outlet of the heat sink. No-slip hydraulic and coupled boundary conditions were imposed on the channel network-coolant interfaces.

4.4. Numerical method

The fluid dynamics and heat transfer modeling were performed using 6SigmaET, which is part of the 6SigmaDCX software package. This

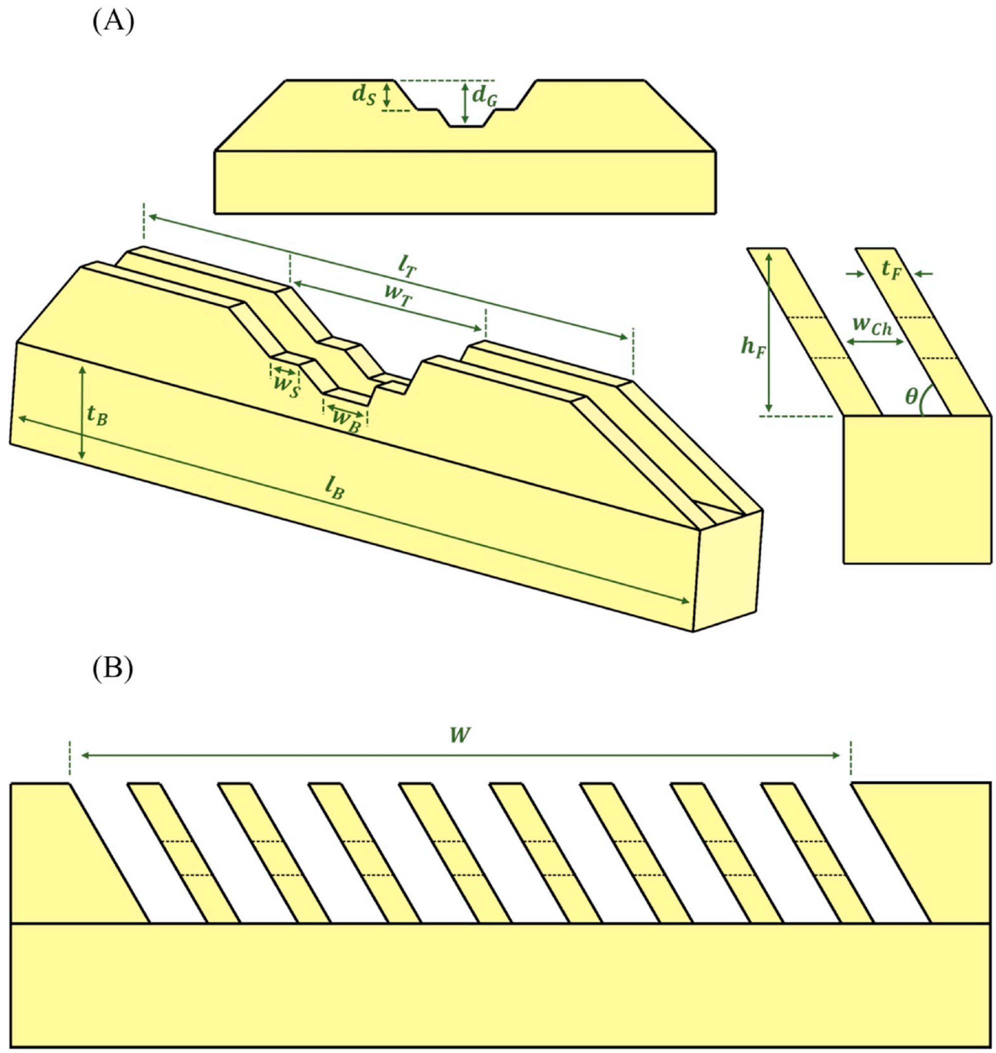

Fig. 4. Geometric parameters of the predefined design (Table 1). (A) A schematic of one channel. (B) A Schematic of heat sink side view shows W sum of the all fins thickness and all channels width.

Table 1
Geometric parameters of the predefined design with their values and definitions.

Symbol	Definition	Value
d_G	Impinging inlet (groove) depth	$0.80mm$
d_s	Depth of the impinging inlet step	$0.69mm$
h_F	Fin height	$1.68mm$
l_B	Channel length at the bottom	$23.56mm$
l_T	Channel length at the top	$18.13mm$
t_B	Base thickness	$1.60mm$
t_F	Fin thickness	$144.00\mu m$
W	Sum of all fins thickness and space	27.11 mm
w_B	Width of the impinging inlet (groove) at the bottom	0.40 mm
w_{Ch}	Channel width	128.50 μm
w_S	Width of the impinging inlet step	73.14 μm
w_T	Width of the impinging inlet (groove) at the top	4.08 mm
θ	Fin tilt angle	63°

Table 2
Thermo-physical properties of the coolant (15% propylene glycol aqueous solution) and solid phase (copper) at 300 K.

	$\mu(kg/m.s)$	$c_p(J/kg.K)$	$k(W/m.K)$	$\rho(kg/m^3)$
Coolant	4033	0.518	1013	0.00149
Copper	380	386	9850	–

Table 3
Dimensionless design parameters and range of variations.

Design Parameters	α	β	σ	γ
Definition	$\frac{t_F}{w_{Ch}}$	$\frac{h_F}{w_{Ch}}$	$\frac{h_G}{h_F}$	$\frac{w_B}{w_T}$
Range of variation	[0.9 1.1]	[12 15]	[0.5 1]	[0 1]

package uses the finite volume method to discretize the system of governing equations (Continuity, Navier-Stokes, and Energy equations) in the computational domain on a staggered grid. The standard $k-\varepsilon$ turbulence model is used to treat the turbulent transport in the distributor and the collector (for high values of flow rate used only for model validation (Fig. 9)). All of the heat sink components (distributor, collector, and micro-channel network) were modelled as a single package. In order to calculating field functions of velocity, pressure, and temperature, the system of governing equations was solved using iterative SIMPLE algorithm.

To accurately capture the pressure drop and heat transfer at this scale, 6SigmaET's MLUS (multi-level unstructured solver) was

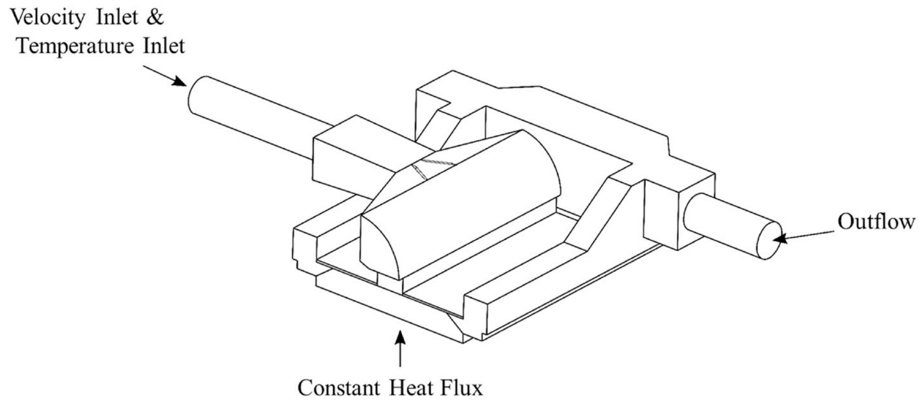

Fig. 5. Computational domain associated with its hydraulic and thermal boundary conditions. All surrounding surfaces are considered as no-slip adiabatic rigid walls.

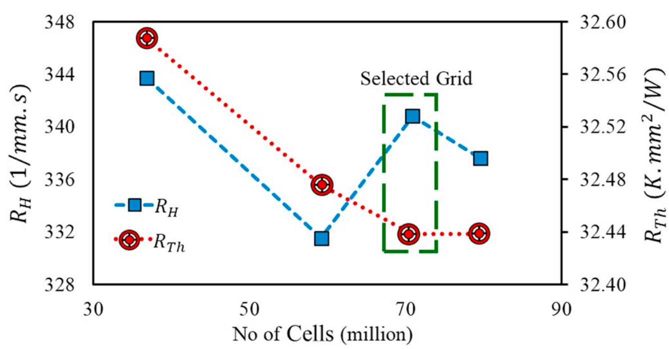

Fig. 6. The results of grid sensitivity analysis based on hydraulic (flow) and thermal resistances (Eqs. (11) and (12)) for predefined design.

employed. The mathematical formulation of this method employs a hierarchy of Cartesian grids and a face-to-cell connectivity graph to discretize the differential equations [67]. The method uses a finite volume scheme with staggered variable arrangement and a pressure-based segregated iteration procedure to solve a discrete algebraic analogue of the equations of motion (Navier-Stocks equations). The method provides accuracy and robustness like the structured procedure and is more flexible in resolving arbitrary geometries and different solution scales. With the unstructured grid providing the necessary resolution of the geometrical details, the model exhibits a substantial reduction in the number of computational cells. The number of cells varies from one design to another owing to fin thickness, space, and impinging inlet geometry. For the predefined and RSM designs (Table 4) this number changes between 70 and 122.5 million depending on the geometry. A grid sensitivity analysis was performed based on the heat sink hydraulic (flow) and thermal resistances defined by Eqs. (11) and (12). The results of this study for the predefined design is illustrated in Fig. 6. By fining the grid from almost 70 millions cell, the hydraulic and thermal resistances show variations less that 1%. While the thermal resistance converges by a descending trend, hydraulic resistance approaches its final value by a fluctuating trend. A grid with almost 70 million cells (specified in Fig. 6) was used for this geometry.

5. Experimental set-up and measurements

Fig. 7 shows a schematic of the experimental apparatus that was used for measuring the heat sink pressure drop, temperature on the base of the heat sink, coolant outlet temperature, and pump power at controlled heat flux, coolant flow rate and inlet temperature. The measured heat sink pressure drop and base temperature were used for calculating the hydraulic and thermal resistances and for validating the numerical model. COP (heat sink coefficient of performance) was calculated at different heat fluxes, coolant flow rates and inlet temperatures using the measured data of pressure drop, and coolant outlet temperature. A copper block with a cross sectional area of 5.588 cm^2 is heated by cartridge heaters powered by a DC (direct current) power supply. Three RTDs (resistance temperature detector) along the copper block measure the temperature gradient to calculate the supplied input power. All sides of the copper block are insulated using fiber wool insulation to ensure that heat is conducted in one dimension to the heat sink. A layer of TIM (thermal interface material) with specified thickness was used to fix the heat sink on the copper block. In order to measure the heat sink base temperature, T-type thermocouples were accommodated in slots machined at two different places on the base of the heat sink (Fig. 8). A gear pump was used to circulate the coolant through the cycle. A chiller unit offering a wide range of operating temperatures was employed to control the coolant inlet temperature. The coolant flow rate was controlled using a micro-flow meter. A micron filter was placed in the cycle to prevent any particles entering the heat sink. The temperature of the coolant at the outlet was measured using a RTD. Finally, a DPT (differential pressure transducer) was used to measure the pressure drop across the heat sink. The data on the measurement uncertainties of the flowmeter, temperature sensors and pressure sensors were obtained from the data sheet (flow meter and pressure) and after a careful in-house calibration of thermocouples (Temperature). The overall uncertainty in the derived quantity is estimated by the propagation of uncertainty. The maximum uncertainty in the heat at 1 lit/min flow rate was estimated to be ±8%. The uncertainty in thermal resistance was estimated as ±6%.

6. Validation of the numerical simulation

The numerical simulations were validated for both the hydraulic and thermal performance by comparing the model results with experimental data for predefined design. Fig. 9 compares the numerical solution and experimental measurements of the predefined design pressure drop (ΔP) for four values of the coolant flow rate. As can be seen, the numerical results are in a good agreement with the experimental data. The maximum and average discrepancies were less than 11% and 7.6%, respectively.

Thermal resistance (R_{Th}), defined as the ratio of the difference in the base temperature (T_B) and coolant inlet temperature (T_{In}) to the electronic chip power ($\dot{q}$), is a reasonable measure for the thermal performance of a single-die heat sink:

$$R_{Th} = \frac{T_B - T_{In}}{\dot{q}} \tag{5}$$

In order to verify the model thermal performance, numerical and experimental data of the predefined design thermal resistance at three

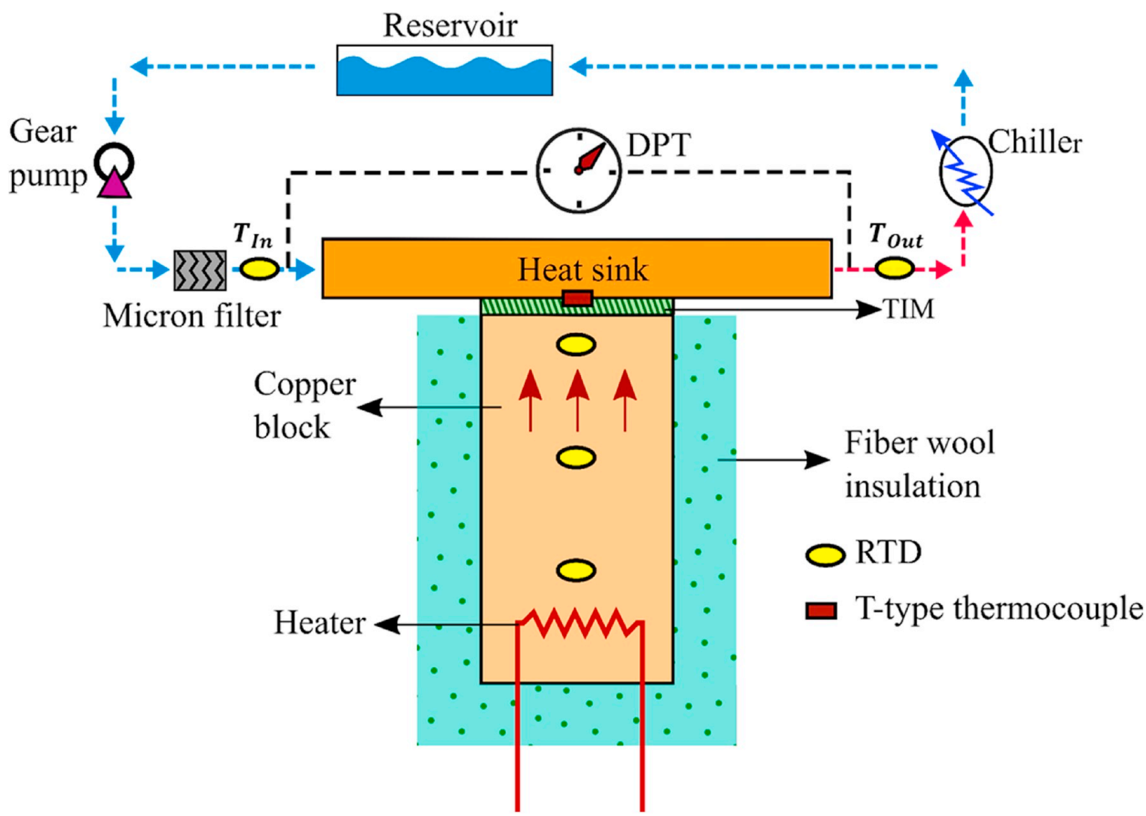

Fig. 7. A schematic illustration of the experimental apparatus used for measuring the heat sink pressure drop, base temperature, and outlet coolant temperature at specified heat flux, coolant flow rate and inlet temperature conditions.

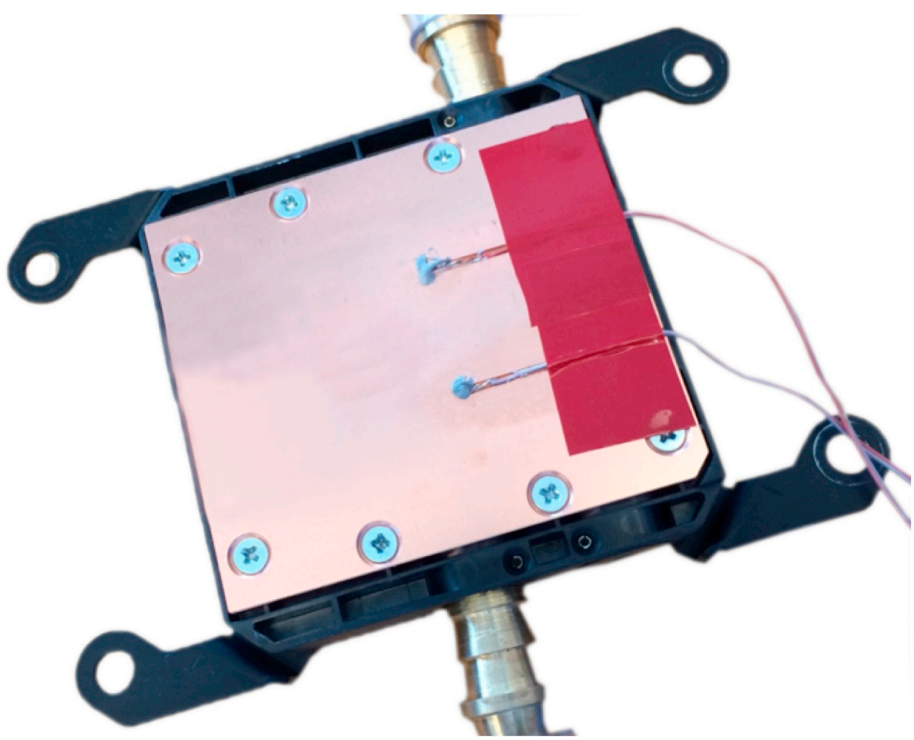

Fig. 8. The position of the T-type thermocouples on the base of the heat sink. The measured temperatures were averaged and used for calculating the thermal resistance of the heat sink.

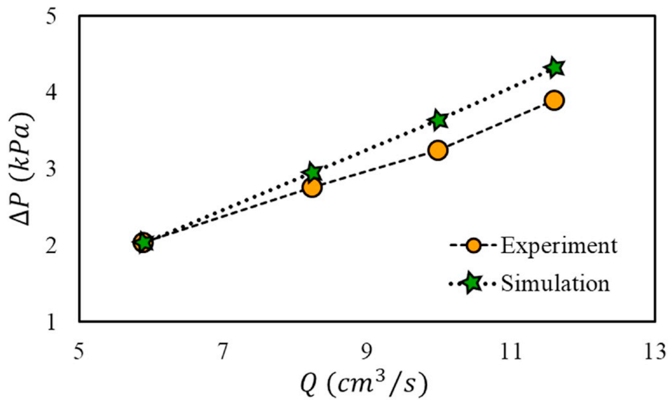

Fig. 9. Comparison of numerical and experimental pressure drop data at four different coolant flow rates for predefined design with an average discrepancy of 7.6%.

coolant flow rates are compared in Fig. 10. As Fig. 10 shows, the experimental data of the thermal resistance are comparable to the model predictions for all values of the coolant flow rate. The maximum and average discrepancies were less than 5% and 2.9%, respectively. It should be mentioned that base temperature (substituted in Eq. (5)) was measured at the two specified points on the base of the heat sink showed in Fig. 8. In the model the base temperature at the same points were calculated and substituted in Eq. (5) for comparison.

7. Optimization

7.1. Fixed parameters

Optimization of the predefined design was done for constant values of electronic chip power (150 W), size (5.588 cm^2), coolant flow rate (5.83 cm^3/s) and inlet temperature (27 °C). The geometric parameters of the heat sink are showed in Fig. 4 and listed in Table 1 associated with their definition and values for predefined design. All of these geometric parameters (showed in Fig. 4 and listed in Table 1) are considered as the geometric fixed parameters, except impinging inlet depth (d_G) and width at the bottom (w_B), fin thickness (t_F), and channel width (w_{Ch}), which are the optimization design parameters. Two changes were made to the geometric parameters of the predefined design. Fins were considered to be vertical ($\theta = 90^\circ$) based on a study [68] that shows vertical fins offer both higher hydraulic and thermal performance. Second, the shape of the impinging inlet cross section was assumed to be a perfect trapezoid. In other word, there is no step ($w_S = 0$) for the impinging inlet. The optimization process is based on the modified predefined design showed in Fig. 11 (A) schematically.

7.2. Design parameters

Fig. 11 (B) shows six geometric parameters for the fins and the impinging inlet that affect the flow and temperature fields. These geometric parameters of the micro-channel network control the hydraulic and thermal performance of the heat sink. Among these six parameters we have to fix the width of impinging inlet at the top, and fin height because of the fixed distributor and collector geometries, respectively. The rest four parameters showed in Fig. 11(B) in red (channel width (w_{Ch}), fin thickness (t_F), impinging inlet depth (d_G), and width at the bottom (w_B)) were considered as the initial design parameters of the optimization process. The following relations can be used for calculating the number of channels and total height of the heat sink (H):

$$t_B + h_F = H \tag{6}$$

$$N w_{Ch} + (N-1) t_F = W \tag{7}$$

Table 4
Calculated response parameters for FCCCD points.

No.	Design Parameters				N	Response Parameters	
	α	β	σ	γ		R_{Th} $(K.mm^2/W)$	R_H $(1/mm.s)$
1	1.00	13.50	0.75	0.50	105	32.97	237.77
2	1.10	12.00	0.50	0.00	89	33.53	207.98
3	0.90	15.00	1.00	1.00	123	33.64	244.87
4	1.00	13.50	1.00	0.50	105	32.97	235.90
5	1.10	12.00	1.00	1.00	89	33.68	194.61
6	1.10	15.00	0.50	1.00	112	32.63	281.76
7	1.00	12.00	0.75	0.50	94	33.01	208.66
8	1.00	13.50	0.75	0.50	105	32.97	237.77
9	1.00	13.50	0.75	0.00	105	33.79	231.50
10	0.90	12.00	1.00	1.00	99	33.01	187.84
11	1.00 13.50	0.75	0.50	105	32.97	237.77	
12	0.90	15.00	1.00	0.00	123	32.37	270.43
13	1.00	13.50	0.75	0.50	105	32.97	237.77
14	1.00	13.50	0.75	0.50	105	32.97	237.77
15	0.90	12.00	0.50	1.00	99	32.89	190.21
16	1.00	13.50	0.75	1.00	105	32.86	221.86
17	0.90	15.00	0.50	0.00	123	32.45	274.83
18	1.10	15.00	0.50	0.00	112	33.01	291.58
19	0.90	12.00	0.50	0.00	99	33.42	191.74
20	0.90	12.00	1.00	0.00	99	33.34	188.35
21	1.10	12.00	0.50	1.00	89	33.75	198.00
22	1.10	15.00	1.00	1.00	112	33.38	273.47
23	1.00	13.50	0.50	0.50	105	33.08	240.14
24	1.00	13.50	0.75	0.50	105	32.97	237.77
25	1.10	12.00	1.00	0.00	89	33.49	208.83
26	0.90	15.00	0.50	1.00	123	32.89	259.43
27	0.90	13.50	0.75	0.50	111	32.86	223.55
28	1.10	15.00	1.00	0.00	112	33.42	279.23
29	1.00	13.50	0.75	0.50	105	32.97	237.77
30	1.10	13.50	0.75	0.50	101	33.75	240.30
31	1.00	15.00	0.75	0.50	117	32.60	278.72

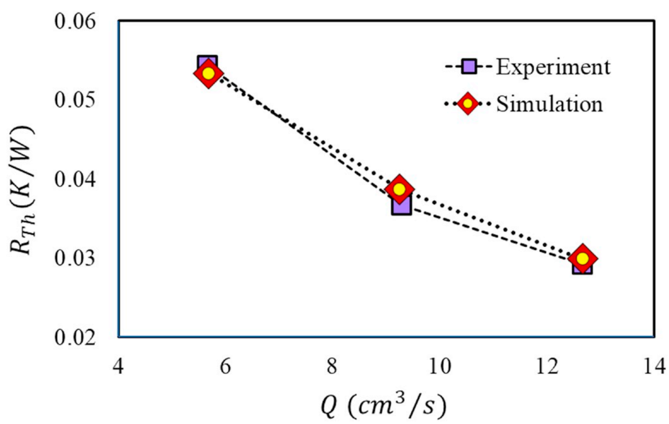

Fig. 10. Comparison of numerical and experimental thermal resistance data at three different values of coolant flow rate for predefined design with an average discrepancy less than 2.9%.

or

$$N = \frac{W + t_F}{w_{Ch} + t_F} \tag{8}$$

where W is the heat sink sum of the all fins thickness and channels width showed in Fig. 4(B). The brackets in Eq. (8) denote the ceiling function. In order to specify the range of variation of the design parameters, we make the quantities dimensionless. The dimensionless design parameters together with their range of variation are listed in Table 3. In terms of the dimensionless design parameters, Eqs. (6) and (8) are rewritten as:

$$\lambda + \phi = 1 \tag{9}$$

$$N = \frac{\omega + \alpha}{\alpha + 1} \tag{10}$$

where $\lambda = \frac{t_B}{H}$, $\phi = \frac{h_F}{H}$ and $\omega = \frac{W}{w_{Ch}}$.

In Table 3, β is the micro-channel aspect ratio. Considering the most common values of β in the available literature for liquid-cooled micro-channel heat sinks [9–11,69–72] and manufacturing constraints a variation range of [12 15] was selected. According to Xie et al. [10] and Upadhye and Kandlikar [73] heat sinks with narrow and deep channels provide lower thermal resistances with a relatively high but acceptable pressure drop. α is the ratio of the fin thickness to fin space (channel width). Common values of α for micro-channel liquid-cooled heat sinks are around 1 [9–13,53,74]. In this study a range of variation of [0.9 1.1] was selected based on manufacturability of the fins ($t_F|_{min} = 0.1\ mm$ for $\alpha = 0.9$ and $\beta = 15$). The groove in the middle of the channels, called impinging inlet, directs the flow to the root of the fins. σ is the ratio of the impinging inlet depth to the fin height. For $\sigma = 1$ the impinging inlet depth is equal to the fin height (maximum depth) and for $\sigma = 0$ the groove vanishes. In comparison to shallow impinging inlets, deep impinging inlets direct the coolant flow to the root of the fins more easily specially when working with narrow channels. A few number of studies [75–77] done on the gas-cooled heat sinks show how a deep impinging inlet helps the flow to reach the root of the fins but in the same time reduce the fluid-solid contact area. Based on previous mentioned studies a range of variation of [0.5 1] was selected for σ. γ is the ratio of the impinging inlet width at the bottom to that at the top. γ specifies the impinging inlet cross section shape. $\gamma = 0$ offers a triangular cross section and $\gamma = 1$ a rectangular cross section. For $0 < \gamma < 1$ the cross section is trapezoidal.

7.3. Response parameters

Thermal resistance (R_{Th}) defined based on chip heat flux and maximum base temperature was considered as a measure of heat sink thermal performance, where:

$$R_{Th} = \frac{T_B^M - T_{In}}{q^{``}} \tag{11}$$

Heat sink hydraulic resistance, measuring pressure drop and hydraulic performance, is defined as:

$$R_H = \frac{\Delta P}{\rho_f Q} \tag{12}$$

where Q is the coolant volumetric flow rate.

7.4. Response surface method

RSM with FCCCD (face centered central composite design) was used to generate 31 design points for four design parameters with three levels. By using CFD (computational fluid dynamics), the response parameters were calculated at the design points. A second order polynomial in the general form of Eq. (13) is employed to approximate the response surface(s).

$$f = a_0 + \sum_{i=1}^{p} a_i X_i + \sum_{i=1}^{p} a_{ii} X_i^2 + \sum_{i<j}^{p} a_{ij} X_i X_j + \varepsilon \tag{13}$$

where a_0 is the intercept, and a_i, a_{ii}, and a_{ij} are the linear, quadratic and interaction coefficients, respectively and ε is the surface error of fitting. The CFD results for the response parameter (hydraulic and thermal resistances) and the number of channels at different RSM design points are showed in Table 4. This table shows that the thermal resistance does not vary significantly at different design points. The selected ranges of variation for the design parameters (Table 3) are not wide enough that cause significant changes in thermal resistance. An additional reason is the negligible effect of the impinging inlet geometry on the thermal performance of the heat sink as showed in Ref. [45]. Therefore, the optimization method is applied to the hydraulic performance of the heat sink in order to minimize its pressure drop.

7.5. Regression and analysis of variance

The calculated regression model for hydraulic resistance is given by Eq. (14) and the corresponding ANOVA (analysis of variance) results are presented in Table 5.

$$\begin{aligned} R_H = {} & 469.00 - 61.50\alpha - 65.50\beta + 63.40\gamma + 58.80\sigma + 3.16\beta^2 - 39.61\gamma^2 \\ & + 10.50\alpha\beta - 2.53\beta\gamma - 5.22\beta\sigma \end{aligned} \tag{14}$$

Table 5 shows that both R^2 and R^2(Adjusted) are very close to one, which verifies the quality of fitting. Close-to-unity R^2(predicted) implies that the calculated regression model is not over-fitted. The terms with P-Values larger than 0.1 were recognized to have insufficient effect on the hydraulic resistance and removed in the regression analysis. In addition to verifying the regression model statistically using analysis of variance, a numerical validation was performed by modeling two intermediate design points. The results of the numerical validation are showed in Table 6. The regression predictions are comparable to the results of the numerical model with a discrepancy less than 3%.

7.6. Effect analysis

The influence of the regression model terms on the hydraulic resistance was calculated using the F-Values of the analysis of variance. The results are showed via a Pareto chart of standardized effects in Fig. 12. As the chart shows, channel aspect ratio (β) has the most significant contribution to the hydraulic resistance of the heat sink. The minimum effect belongs to the interaction of aspect ratio and the ratio of the fin

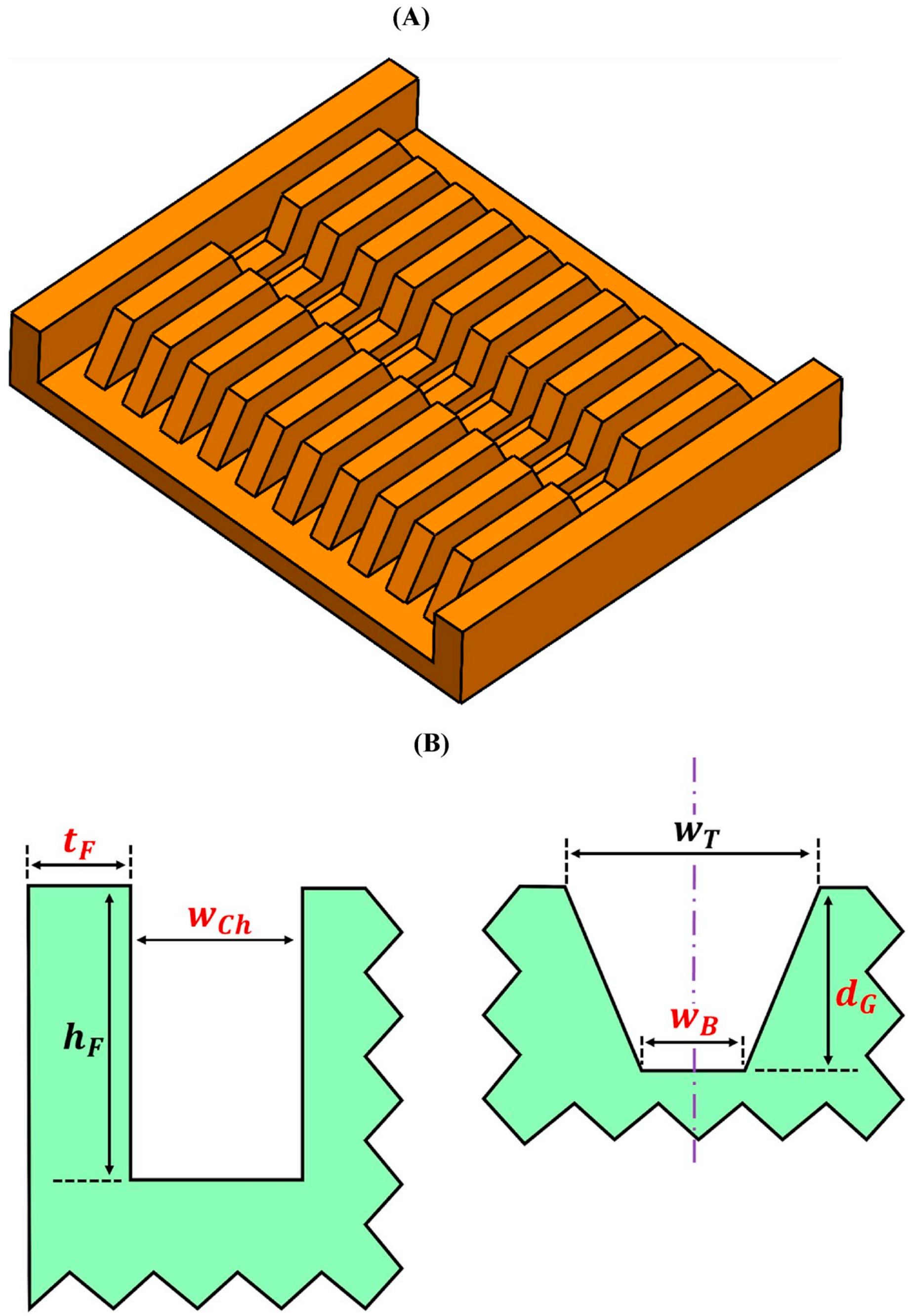

Fig. 11. (A) A Schema of simplified geometry for optimization. (B) Geometric parameters of the fins and impinging inlet. Fin thickness (t_F), channel width (w_{Ch}), impinging depth (d_G) and width at the bottom (w_B) are design parameters. Impinging inlet width at the top (w_T) and fin height (h_F) has to be fixed because of fixed distributor and collector geometries.

thickness to the channel width. A Pareto chart of standardized effects displays the intensity of the effects. However, it does not show the direction of the effects. For example, a parameter has a positive effect if the response parameter increases by increasing it and vice versa. In order to determine how the design parameters affect the response parameters, a parametric study was performed based on the numerical results at RSM design points.

7.7. Parametric study

A parametric study was conducted for the design parameters to estimate their effects on the hydraulic and thermal resistances. This study was done based on the current operational and geometrical fixed parameters and for the entire heat sink package including distributor and collector.

7.7.1. Impinging inlet

The effect of the impinging inlet geometry on the hydraulic resistance is illustrated in Fig. 13 (A). Increasing the depth of the impinging inlet (σ) slightly decreases the hydraulic resistance. By increasing σ, liquid-solid contact surface area decreases, that reduces the flow friction and minor losses.

It is also showed that, there is a small increase in hydraulic resistance when the shape of the impinging inlet deviates from a triangle. The maximum hydraulic resistance is at $\gamma = 0.4$. The minimum value of hydraulic resistance is achieved for a rectangular cross section.

Table 5
ANOVA results for hydraulic resistance.

Source	DOF	Adj. SS	Adj. MS	F-Value	P-Value
Model	9	27830.1	3092.2	256.71	0.000
Linear	4	27331.3	6832.8	567.25	0.000
α	1	1160.2	1160.2	96.32	0.000
β	1	25545.5	25545.5	2120.76	0.000
γ	1	474.5	474.5	39.39	0.000
σ	1	151.0	151.0	12.54	0.002
Square	2	340.6	170.3	14.14	0.000
β^2	1	175.2	175.2	14.55	0.001
γ^2	1	340.3	340.3	28.26	0.000
2-Way Interaction	3	158.3	52.8	4.38	0.015
$\alpha\beta$	1	39.7	39.7	3.30	0.084
$\beta\gamma$	1	57.4	57.4	4.76	0.041
$\beta\sigma$	1	61.2	61.2	5.08	0.035
Error	21	253.0	12.0	–	–
Lack- of -Fit	15	253.0	16.9	–	–
Pure Error	6	0.0	0.0	–	–
Total	30	28083.1	–	–	–
Standard Deviation		R^2	R^2(Adjusted)	R^2(Predicted)	
3.47065		99.10%	98.71%	97.33%	

Table 6
Regression model verification by CFD results of intermediate points.

Design Parameters				$R_H(1\ /mm.s)$		
α	β	σ	γ	Simulation	Regression	Discrepancy
0.95	14.5	0.90	0.75	256.21	252.00	1.65%
1.05	13.0	0.60	0.25	236.07	229.67	2.71%

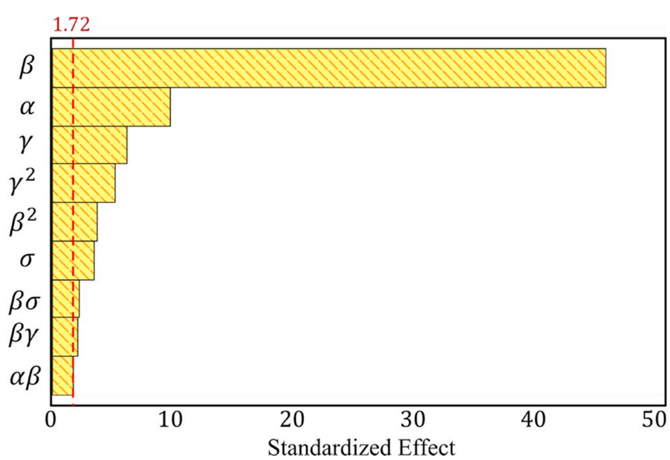

Fig. 12. Pareto chart of standardized effects. Channel aspect ratio has the most significant contribution to the hydraulic resistance.

Variation in thermal resistance with impinging inlet geometry is showed in Fig. 13 (B). An impinging inlet with rectangular cross section ($\gamma = 1$) and high depth ($\sigma \approx 1$) improve thermal performance because it helps the flow to penetrate to the root of the fins easily.

7.7.2. Fin and channel

The influence of fin and channel geometry on the hydraulic performance of the heat sink is showed in Fig. 14 (A). The hydraulic resistance increases by increasing the ratio of fin thickness to channel width (α) at constant channel aspect ratio (β). For increasing α at constant β, one has to fix channel width (h_F is constant) and increase fin thickness. With increasing the fin thickness at fixed channel width, we decrease the number of channels (Eq. (8) $\rightarrow \left.\frac{\partial N}{\partial t_F}\right|_{w_{Ch}} < 0$), resulting in higher coolant velocity through the channels and increasing hydraulic resistance.

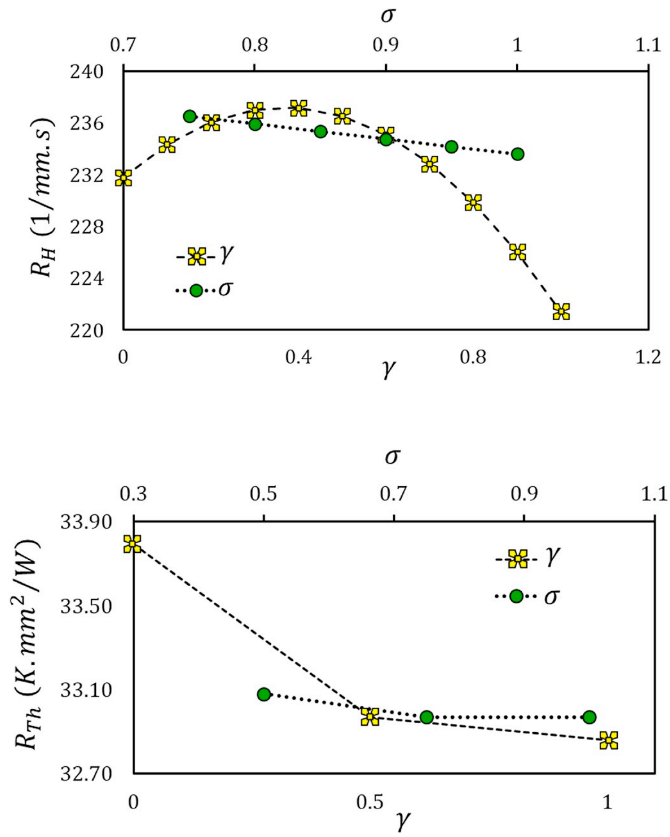

Fig. 13. The effect of impinging inlet on the response parameters (A) R_H and (B) R_{Th} in constant coolant flow rate and heat sink width (σ at $\alpha = 1$, $\beta = 13.5$, and $\gamma = 0.5$ as well as γ at $\alpha = 1$, $\beta = 13.5$, and $\sigma = 0.75$).

Fig. 14 (A) shows that the heat sink hydraulic resistance increases dramatically by increasing channels aspect ratio (β). First, it is difficult for the flow to enter the deep and narrow channels from the top when it exits the distributor. Second, narrow channels possess small hydraulic diameters that provide higher liquid-solid contact area and coolant velocity resulting in increasing the friction significantly. By decreasing the channel width (increasing β) at constant α the number of channels increases that reduces the coolant velocity. However, the effect of hydraulic diameter dominates. The results obtained in this study for the effect of channel aspect ratio on the hydraulic resistance are in agreement with the results for parallel flow heat sinks [10].

Fig. 14 (B) illustrates the influence of channel geometry on the heat sink thermal resistance. Increasing α increase thermal resistance because it decreases the number of channels and reduces solid-liquid contact area. Increasing channel aspect ratio (β) improves heat sink thermal performance because deep channels provide more heat transfer (liquis-solid) surface area.

7.7.3. Optimal design

The optimal design was obtained by minimizing the hydraulic resistance regression model of Eq. (14) for the design parameters selected ranges of variation (Table 3) using iterative JAYA algorithm [78]. The calculated dimensionless and initial design parameters for the optimal design are showed in Table 7. By optimizing the predefined design, the hydraulic resistance was reduced by 45% without a significant increase in thermal resistance (1.6%). Fig. 15 compares the hydraulic and thermal performance of the predefined and optimal designs. The same amount of reduction (45%) was achieved in pump power

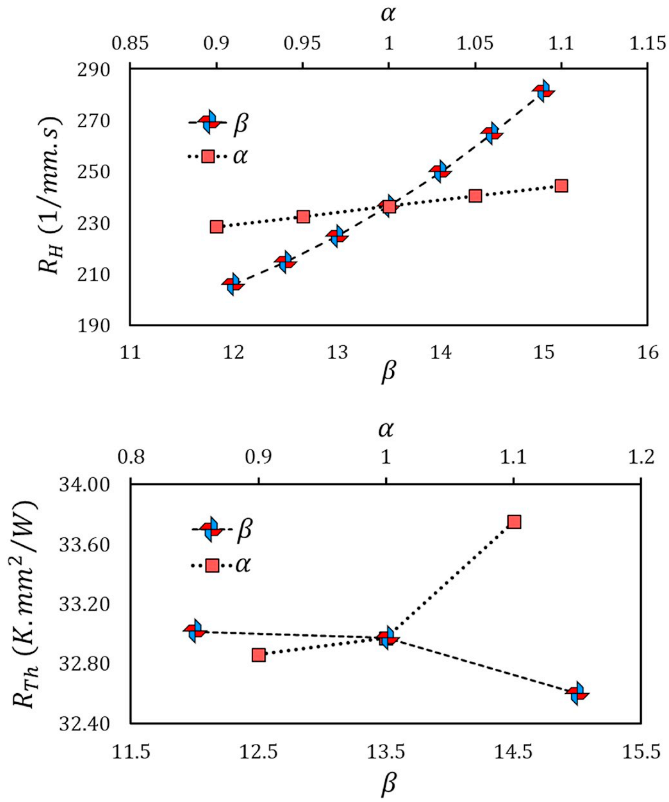

Fig. 14. The effect of the channel geometry on the response parameters (A) R_H and (B) R_{Th} in constant coolant flow rate and heat sink width (α at $\beta = 13.5$, $\gamma = 0.5$, and $\sigma = 0.75$ as well as β at $\alpha = 1$, $\gamma = 0.5$, and $\sigma = 0.75$).

Table 7
Dimensionless and initial design parameters of optimal (minimum hydraulic resistance) design.

Dimensionless Design Parameters			
α	β	σ	γ
0.9	12	1.0	1.0
Initial Design Parameters (mm)			
t_F	w_{Ch}	d_G	w_B
0.126	0.140	1.680	4.080

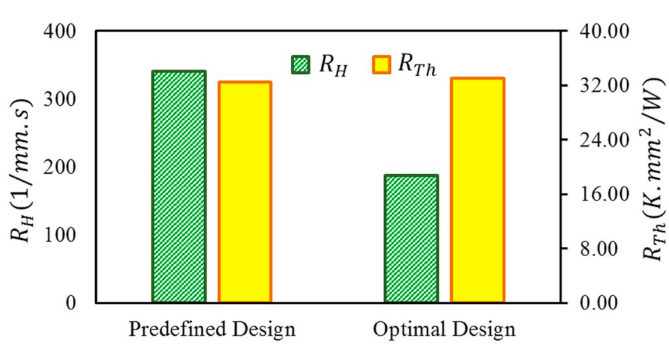

Fig. 15. A comparison between the predefined and optimal designs based on thermal and hydraulic performance.

because the optimization was performed for constant flow rate ($\dot{w}_P = Q^2 R_H$). Finally, an increase of 9% in the fin gap makes the manufacturing process more straightforward.

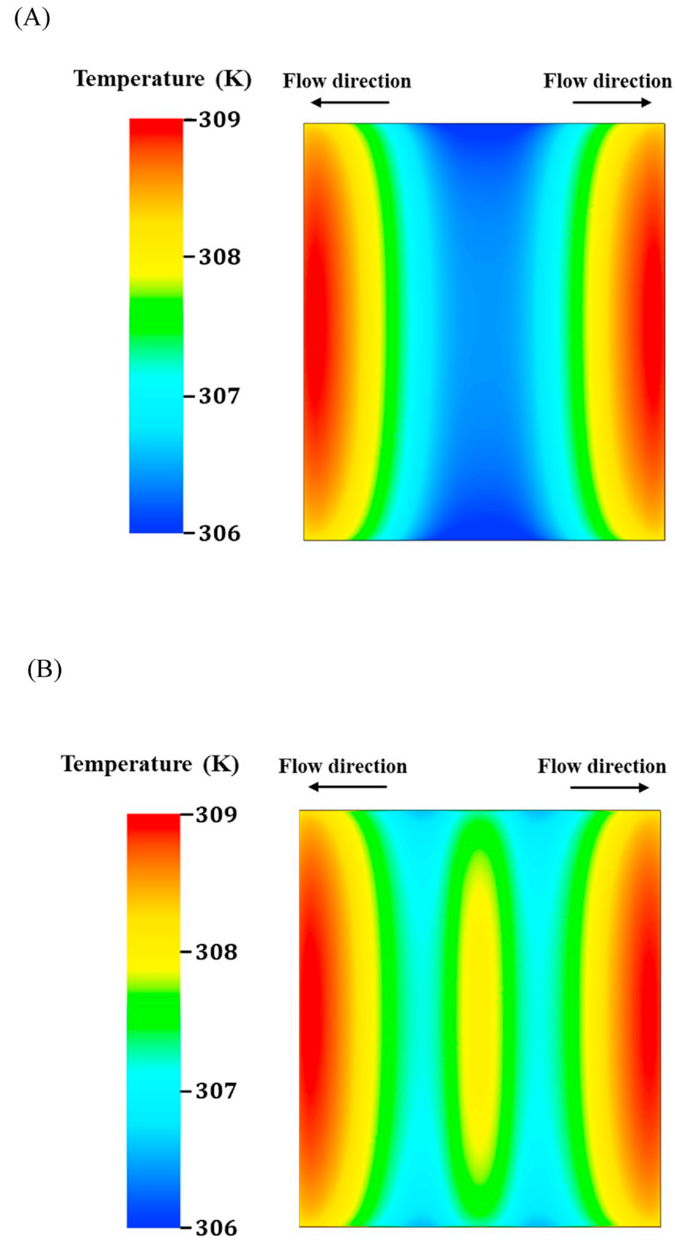

Fig. 16. Chip-base interface (junction) temperature profile. (A) When σ and γ are not equal to one simultaneously (design point 28 in Table 4). (B) When $\sigma = \gamma = 1$ (design point 22 in Table 4) and a stagnation zone formed a long the impinging inlet.

8. Chip-base temperature profile

In parallel channel heat sinks, the chip-base interface temperature reaches it maximum at the center of the chip and decreases closer to the edges. However, in impingement heat sinks, due to the different flow field, the chip-base (junction) temperature profile is totally different. Fig. 16 (A) shows the temperature profile on the chip-base interface of model number 28 in Table 4. The minimum temperature region lies under the impinging inlet. By moving along the channels in the direction of the flow, the interface temperature increases and is a maximum near the edges at the channels exit. Similar temperature profiles are obtained for the predefined design and for other designs showed in Table 4, except for those that σ and γ are simultaneously equal to unity. For the designs with $\sigma = \gamma = 1$, the impinging inlet has a rectangular cross section with a width equal to the width of the diffuser and a depth equals to the fin height. This geometry for the impinging inlet creates a wide

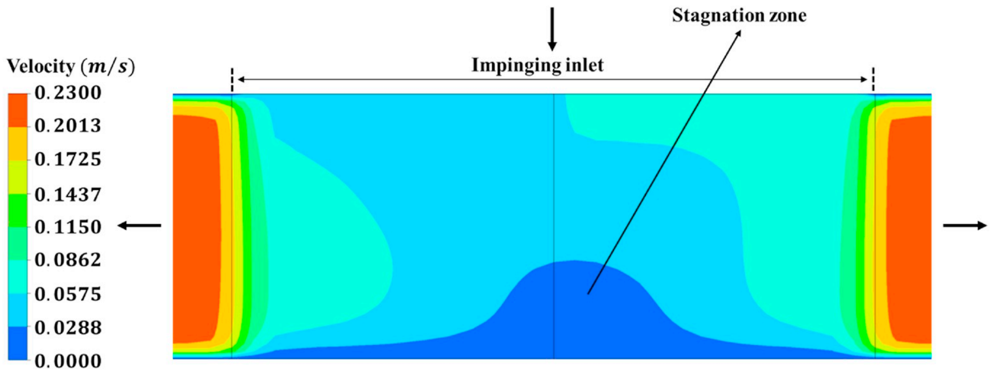

Fig. 17. Velocity profile in symmetry plane of a channel shows the cross section of the stagnation zone formed along the impinging inlet for the design point of 22 ($\sigma = \gamma = 1$).

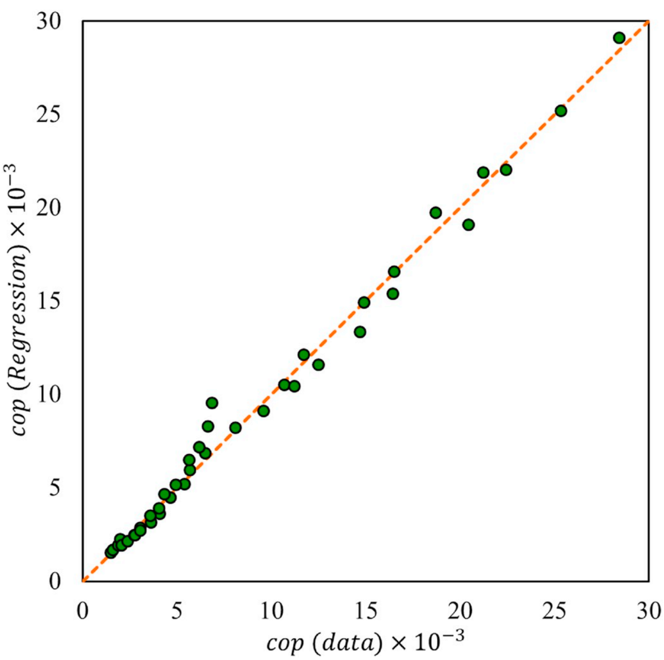

Fig. 18. Parity plot of the *cop* regression model verifies the quality of fitting.

stagnation zone. The cross section of this stagnation zone is showed in Fig. 17. This stagnation zone attenuates the heat transfer in the impinging inlet and causes that the chip temperature to increase in the region below it. Fig. 16 (B) shows the effect of this geometry of the impinging inlet on the junction temperature profile.

9. Coefficient of performance sensitivity analysis

COP (coefficient of performance) measures the heat sink thermo-hydraulic performance and comprises the influence of the coolant temperature on the pressure drop and pump power. In designing the heat sinks, it is useful to have an estimation of the heat sink coefficient of performance before identifying the operational parameters (coolant flow rate and inlet temperature, chip power, pump power, etc.) and fixing their values. The coefficient of performance is the ratio of heat removed by the heat sink from the chip to the pump power. Therefore, it includes both hydraulic and thermal contributions:

$$cop = \frac{\dot{q}}{\dot{w}_P} \tag{15}$$

where $\dot{q}$ is the heat removed by the coolant that is equal to the electronic chip power in the ideal conditions (when all of the generated heat is removed by the heat sink) and $\dot{w}_P$ is the pump power. In this study, the COP of the predefined design was calculated at different measured values of operational parameters: chip power and coolant flow rate and inlet temperature. A regression model was developed based on the calculated COP data:

$$COP = exp(0.007954\ \dot{q} + 0.01928\ T_{In} + 0.2475\ Q - 0.4169) \tag{16}$$

for

$$70\ W \le \dot{q} \le 210\ W$$

$$6\ cm^3/s \le Q \le 12\ cm^3/s$$

$$298\ K \le T_{In} \le 318\ K$$

The coefficient regression (R^2) is estimated to be 98.9%. Fig. 18 shows the parity plot of the regression. As can be seen, the scatter of the points is very close to the actual data that confirms a high quality of fitting.

A sensitivity analysis was performed to determine the influence of

Table 8
Sensitivity analysis of the COP.

$\dot{q}(W)$	$T_{in}(K)$	$Q(cm^3/s)$	$\frac{\partial COP}{\partial \dot{q}}$	$\frac{\partial COP}{\partial T_{in}}$	$\frac{\partial COP}{\partial Q}$
70	298	6	12.63	30.62	393.07
70	308	6	15.32	37.13	476.65
70	318	6	18.58	45.03	578.00
140	298	6	22.04	53.43	685.92
140	308	6	26.73	64.79	831.77
140	318	6	32.41	78.57	1008.64
210	298	6	38.47	93.24	1196.95
210	308	6	46.65	113.07	1451.47
210	318	6	56.57	137.11	1760.12
70	298	9	26.54	64.34	825.90
70	308	9	32.19	78.02	1001.52
70	318	9	39.03	94.61	1214.48
140	298	9	46.32	112.27	1441.23
140	308	9	56.17	136.14	1747.70
140	318	9	68.11	165.09	2119.33
210	298	9	80.83	195.92	2515.02
210	308	9	98.01	237.58	3049.81
210	318	9	118.85	288.10	3698.33
70	298	12	55.77	135.18	1735.37
70	308	12	67.63	163.93	2104.38
70	318	12	82.01	198.79	2551.85
140	298	12	97.32	235.90	3028.30
140	308	12	118.02	286.06	3672.23
140	318	12	143.11	346.89	4453.10
210	298	12	169.83	411.66	5284.51
210	308	12	205.94	499.19	6408.21
210	318	12	249.73	605.34	7770.85

the input parameters on the output variable. The effective parameters are ranked in order of influence by using the results of the sensitivity analysis. The partial derivatives of the COP with respect to $\dot{q}$, T_{In}, and Q are calculated as the sensitivity of the output parameter with respect to those effective parameters [79]:

$$\frac{\partial COP}{\partial \dot{q}} = 0.007954\ \exp(0.007954\ \dot{q} + 0.01928\ T_{In} + 0.2475\ Q - 0.4169) \tag{17}$$

$$\frac{\partial COP}{\partial T_{In}} = 0.01928\ \exp(0.007954\ \dot{q} + 0.01928\ T_{In} + 0.2475\ Q - 0.4169) \tag{18}$$

$$\frac{\partial COP}{\partial Q} = 0.2475\ \exp(0.007954\ \dot{q} + 0.01928\ T_{In} + 0.2475\ Q - 0.4169) \tag{19}$$

A positive sensitivity value indicates that the output parameter increases by an increment in the input parameters and vice versa. The results of sensitivity analysis obtained from Eqs. (17)–(19) are showed in Table 8. According to Table 8, it can be concluded that:

- The sensitivity of the COP to chip power is positive. By increasing the chip power, the temperature gradient (heat transfer potential) increases. This sensitivity increases with increasing coolant temperature and flow rate and chip power.
- The sensitivity of the COP to coolant inlet temperature is positive. This means COP increases by increasing inlet coolant temperature. Increasing the coolant inlet temperature decreases the temperature gradient (heat transfer potential), however the coolant viscosity decreases which reduces the pump work. This sensitivity increases with increment in chip power and coolant flow rate and inlet temperature.
- The sensitivity of the COP to coolant flow rate is positive. By increasing the coolant flow rate, the pump work is increased, but the velocity in the channels also increases and enhances the convective heat transfer. The effect of flow rate change on heat transfer is larger than that on pump power due to the high ability of water to store and carry the heat ($\rho c_p|_{\text{Water}} \gg 1$). The results of Table 8 show that the sensitivity of COP to flow rate increases by increasing all three effective parameters.
- The sensitivity of COP to coolant flow rate is at least one order of magnitude larger than the other two effective parameters. Therefore coolant flow rate is the dominant parameter in controlling the heat sink COP.

10. Conclusion

Water-cooled impingement heat sinks are preferred over parallel flow heat sink due to their lower pressure drop when there is no space restriction and coolant can enter perpendicular to the electronic board. A numerical model including distributor and collector was developed to calculate the performance and optimize the shape of a commercial water-cooled impingement heat sink. The major conclusion from the numerical study is as follows

(I) In consonance with optimization results, it is evident that the pressure drop reduces by 45% without a significant change in thermal performance. Furthermore, the results of the effect analysis show that, channel aspect ratio has the most significant contribution to the pressure drop.
(II) Parametric study reveals that the channel geometry plays a more effective role in heat sink pressure drop than the impinging inlet geometry.
(III) The chip-base interface temperature profile obtained (for constant chip heat flux) numerically showed that the chip temperature reaches its maximum near the edges at the channel exit.
(IV) A sensitivity analysis was performed for heat sink coefficient of performance which shows that it is most sensitive to coolant flow rate.
(V) The optimized heat sink corresponds to COP enhanced by 80% from the predefined design.

Acknowledgment

This work is supported by NSF IUCRC Award No. IIP-1738793. The authors would like to acknowledge Mark Seymour from Future Facilities, Steven Schon from QuantaCool, Tom Carft from Commscope, and Russ Tipton from Vertiv Co for their useful comments and guidance through the course of this study.

References

[1] D.B. Tuckerman, R.F.W. Pease, High-performance heat sinking for VLSI, IEEE Electron. Device Lett. 2 (1981) 126–129, https://doi.org/10.1109/EDL.1981.25367.
[2] W. Qu, I. Mudawar, Experimental and numerical study of pressure drop and heat transfer in a single-phase micro-channel heat sink, Int. J. Heat Mass Transf. 45 (2002) 2549–2565.
[3] H.Y. Zhang, D. Pinjala, T.N. Wong, K.C. Toh, Y.K. Joshi, Single-phase liquid cooled microchannel heat sink for electronic packages, Appl. Therm. Eng. 25 (2005) 1472–1487.
[4] Y.P. Zhang, X.L. Yu, Q.K. Feng, R.T. Zhang, Thermal performance study of integrated cold plate with power module, Appl. Therm. Eng. 29 (2009) 3568–3573.
[5] M. Reyes, J.R. Arias, A. Velazquez, J.M. Vega, Experimental study of heat transfer and pressure drop in micro-channel based heat sinks with tip clearance, Appl. Energy 31 (2011) 887–893.
[6] D. Liu, Suresh V. Gaimella, Analysis and optimization of the thermal performance of microchannel heat sinks, Int. J. Numer. Methods Heat Fluid Flow 15 (2004) 7–26.
[7] G. Turkakar, T.O. Ozyurt, Dimensional optimization of microchannel heat sinks with multiple heat sources, Int. J. Therm. Sci. 62 (2012) 85–92.
[8] J. Cruz, I. Amaya, R. Correa, Optimal rectangular microchannel design, using simulated annealing, unified particle swarm and spiral algorithms, in the presence of spreading resistance, Appl. Energy 84 (2015) 126–137.
[9] X.L. Xie, W.Q. Tao, Y.L. He, Numerical study of turbulent heat transfer and pressure drop characteristics in a water-cooled minichannel heat sink, J. Electron. Packag. 129 (2006) 247–255, https://doi.org/10.1115/1.2753887.
[10] X.L. Xie, Z.J. Liu, Y.L. He, W.Q. Tao, Numerical study of laminar heat transfer and pressure drop characteristics in a water-cooled minichannel heat sink, Appl. Therm. Eng. 29 (2009) 64–74, https://doi.org/10.1016/j.applthermaleng.2008.02.002.
[11] X.H. Yang, S.C. Tan, Y.J. Ding, J. Liu, in: Flow and thermal modeling and optimization of micro/mini-channel heat sink, 117, 2017, pp. 289–296.
[12] H. Ermagan, R. Rafee, Geometric optimization of an enhanced microchannel heat sink with superhydrophobic walls, Appl. Therm. Eng. 130 (2018) 384–394, https://doi.org/10.1016/j.applthermaleng.2017.11.039.
[13] L. Lin, Y.Y. Chen, X.X. Zhang, X.D. Wang, Optimization of geometry and flow rate distribution for double-layer microchannel heat sink, Int. J. Therm. Sci. 78 (2014) 158–168.
[14] K. Kulkarni, A. Afzal, K.Y. Kim, Multi-objective optimization of a double-layered microchannel heat sink with temperature-dependent fluid properties, Appl. Therm. Eng. 99 (2016) 262–272.
[15] Y.F. Li, G.D. Xia, D.D. Ma, Y.T. Jia, J. Wang, Characteristics of laminar flow and heat transfer in microchannel heat sink with triangular cavities and rectangular ribs, Int. J. Heat Mass Transf. 98 (2016) 17–28, https://doi.org/10.1016/j.ijheatmasstransfer.2016.03.022.
[16] G. Xia, Y. Zhai, Z. Cui, Numerical investigation of thermal enhancement in a micro heat sink with fan-shaped reentrant cavities and internal ribs, Appl. Therm. Eng. 58 (2013) 52–60, https://doi.org/10.1016/j.applthermaleng.2013.04.005.
[17] L. Chai, G.D. Xia, H.S. Wang, Parametric study on thermal and hydraulic characteristics of laminar flow in microchannel heat sink with fan-shaped ribs on sidewalls – Part 2: pressure drop, Int. J. Heat Mass Transf. 97 (2016) 1081–1090, https://doi.org/10.1016/j.ijheatmasstransfer.2016.02.076.
[18] L. Chai, G.D. Xia, H.S. Wang, Parametric study on thermal and hydraulic characteristics of laminar flow in microchannel heat sink with fan-shaped ribs on sidewalls – Part 1: heat transfer, Int. J. Heat Mass Transf. 97 (2016) 1069–1080, https://doi.org/10.1016/j.ijheatmasstransfer.2016.02.077.
[19] L. Chai, G.D. Xia, H.S. Wang, Parametric study on thermal and hydraulic characteristics of laminar flow in microchannel heat sink with fan-shaped ribs on sidewalls – Part 3: performance evaluation, Int. J. Heat Mass Transf. 97 (2016) 1091–1101, https://doi.org/10.1016/j.ijheatmasstransfer.2016.02.075.
[20] G. Xie, J. Liu, W. Zhang, B. Sunden, Analysis of flow and thermal performance of a water-cooled transversal wavy microchannel heat sink for chip cooling, J. Electron. Packag. 134 (2012), https://doi.org/10.1115/1.4023035, 041010-041010–6.
[21] W. Duangthongsuk, S. Wongwises, A comparison of the thermal and hydraulic performances between miniature pin fin heat sink and microchannel heat sink with

zigzag flow channel together with using nanofluids, Heat Mass Transf. 54 (2018) 3265–3274, https://doi.org/10.1007/s00231-018-2370-y.
[22] Y. Xie, Z. Shen, D. Zhang, J. Lan, Thermal performance of a water-cooled microchannel heat sink with grooves and obstacles, J. Electron. Packag. 136 (2014), https://doi.org/10.1115/1.4025757, 021001-021001–8.
[23] Y. Li, F. Zhang, B. Sunden, G. Xie, Laminar thermal performance of microchannel heat sinks with constructural vertical Y-shaped bifurcation plates, Appl. Therm. Eng. 73 (2014) 185–195, https://doi.org/10.1016/j.applthermaleng.2014.07.031.
[24] G. Xie, F. Zhang, B. Sundén, W. Zhang, Constructal design and thermal analysis of microchannel heat sinks with multistage bifurcations in single-phase liquid flow, Appl. Therm. Eng. 62 (2014) 791–802, https://doi.org/10.1016/j.applthermaleng.2013.10.042.
[25] G. Xie, S. Li, B. Sunden, W. Zhang, H. Li, A numerical study of the thermal performance of microchannel heat sinks with multiple length bifurcation in laminar liquid flow, Numer. Heat Transf., Part A: Applications 65 (2014) 107–126, https://doi.org/10.1080/10407782.2013.826084.
[26] V. SARAVANAN, C.K. UMESH, Numerical comparison for thermo-hydraulic performance of pin fin heat sink with micro channel pin fin heat sink, Sādhanā. 43 (2018) 100, https://doi.org/10.1007/s12046-018-0875-1.
[27] J. Xie, H. Yan, B. Sundén, G. Xie, The influences of sidewall proximity on flow and thermal performance of a microchannel with large-row pin-fins, Int. J. Therm. Sci. 140 (2019) 8–19, https://doi.org/10.1016/j.ijthermalsci.2019.02.031.
[28] S. Huang, J. Zhao, L. Gong, X. Duan, Thermal performance and structure optimization for slotted microchannel heat sink, Appl. Therm. Eng. 115 (2017) 1266–1276, https://doi.org/10.1016/j.applthermaleng.2016.09.131.
[29] A. Ghahremannezhad, K. Vafai, Thermal and hydraulic performance enhancement of microchannel heat sinks utilizing porous substrates, Int. J. Heat Mass Transf. 122 (2018) 1313–1326, https://doi.org/10.1016/j.ijheatmasstransfer.2018.02.024.
[30] A. Ghahremannezhad, H. Xu, M. Alhuyi Nazari, M. Hossein Ahmadi, K. Vafai, Effect of porous substrates on thermohydraulic performance enhancement of double layer microchannel heat sinks, Int. J. Heat Mass Transf. 131 (2019) 52–63, https://doi.org/10.1016/j.ijheatmasstransfer.2018.11.040.
[31] H.-C. Chiu, R.-H. Hsieh, K. Wang, J.-H. Jang, C.-R. Yu, The heat transfer characteristics of liquid cooling heat sink with micro pin fins, Int. Commun. Heat Mass Transf. 86 (2017) 174–180, https://doi.org/10.1016/j.icheatmasstransfer.2017.05.027.
[32] D. Yang, Y. Wang, G. Ding, Z. Jin, J. Zhao, G. Wang, Numerical and experimental analysis of cooling performance of single-phase array microchannel heat sinks with different pin-fin configurations, Appl. Therm. Eng. 112 (2017) 1547–1556, https://doi.org/10.1016/j.applthermaleng.2016.08.211.
[33] F.M. White, Fluid Mechanics, eighth ed., McGraw Hill Education, New York, USA, 2016.
[34] Y. Zhuang, C.F. Ma, M. Qin, Experimental study on local heat transfer with liquid impingement flow in two-dimensional micro-channels, Int. J. Heat Mass Transf. 40 (1997) 4055–4059, https://doi.org/10.1016/S0017-9310(97)00039-2.
[35] D. Lelea, Effects of inlet geometry on heat transfer and fluid flow of tangential micro-heat sink, Int. J. Heat Mass Transf. 53 (2010) 3562–3569, https://doi.org/10.1016/j.ijheatmasstransfer.2010.04.018.
[36] D. Lelea, The tangential micro-heat sink with multiple fluid inlets, Int. Commun. Heat Mass Transf. 39 (2012) 190–195, https://doi.org/10.1016/j.icheatmasstransfer.2011.12.005.
[37] M. Iyengar, M. Ellsworth, Design and analysis of direct liquid multi-jet impingement schemes for electronics applications, in: American Society of Mechanical Engineers, 2004, pp. 249–256, https://doi.org/10.1115/IMECE2004-61495.
[38] P. Naphon, S. Klangchart, Effects of outlet port positions on the jet impingement heat transfer characteristics in the mini-fin heat sink, Int. Commun. Heat Mass Transf. 38 (2011) 1400–1405, https://doi.org/10.1016/j.icheatmasstransfer.2011.08.017.
[39] S. Wiriyasart, P. Naphon, Liquid impingement cooling of cold plate heat sink with different fin configurations: high heat flux applications, Int. J. Heat Mass Transf. 140 (2019) 281–292, https://doi.org/10.1016/j.ijheatmasstransfer.2019.06.020.
[40] R. Chein, J. Chuang, Experimental microchannel heat sink performance studies using nanofluids, Int. J. Therm. Sci. 46 (2007) 57–66, https://doi.org/10.1016/j.ijthermalsci.2006.03.009.
[41] L. Nakharintr, P. Naphon, Magnetic field effect on the enhancement of nanofluids heat transfer of a confined jet impingement in mini-channel heat sink, Int. J. Heat Mass Transf. 110 (2017) 753–759, https://doi.org/10.1016/j.ijheatmasstransfer.2017.03.078.
[42] P. Naphon, S. Wiriyasart, Experimental study on laminar pulsating flow and heat transfer of nanofluids in micro-fins tube with magnetic fields, Int. J. Heat Mass Transf. 118 (2018) 297–303, https://doi.org/10.1016/j.ijheatmasstransfer.2017.10.131.
[43] L. Nakharintr, P. Naphon, S. Wiriyasart, Effect of jet-plate spacing to jet diameter ratios on nanofluids heat transfer in a mini-channel heat sink, Int. J. Heat Mass Transf. 116 (2018) 352–361, https://doi.org/10.1016/j.ijheatmasstransfer.2017.09.037.
[44] P. Naphon, L. Nakharintr, S. Wiriyasart, Continuous nanofluids jet impingement heat transfer and flow in a micro-channel heat sink, Int. J. Heat Mass Transf. 126 (2018) 924–932, https://doi.org/10.1016/j.ijheatmasstransfer.2018.05.101.
[45] Y. Hadad, R. Pejman, B. Ramakrishnan, P.R. Chiarot, B.G. Sammakia, Geometric optimization of an impinging cold-plate with a trapezoidal groove used for warm water cooling, in: 2018 17th IEEE Intersociety Conference on Thermal and Thermomechanical Phenomena in Electronic Systems, ITherm), 2018, pp. 673–682, https://doi.org/10.1109/ITHERM.2018.8419540.
[46] J.M. Commenge, L. Falk, J.P. Corriou, M. Matlosz, Optimal design for flow uniformity in microchannel reactors, AIChE J. 48 (2002) 345–358, https://doi.org/10.1002/aic.690480218.
[47] J.H. Ryu, D.H. Choi, S.J. Kim, Three-dimensional numerical optimization of a manifold microchannel heat sink, Int. J. Heat Mass Transf. 46 (2003) 1553–1562, https://doi.org/10.1016/S0017-9310(02)00443-X.
[48] O. Tonomura, S. Tanaka, M. Noda, M. Kano, S. Hasebe, I. Hashimoto, CFD-based optimal design of manifold in plate-fin microdevices, Chem. Eng. J. 101 (2004) 397–402, https://doi.org/10.1016/j.cej.2003.10.022.
[49] D. Bogojevic, K. Sefiane, A.J. Walton, J.R.E. Christy, G. Cummins, H. Lin, Investigation of flow distribution in microchannels heat sinks, Heat Transf. Eng. 30 (2009) 1049–1057, https://doi.org/10.1080/01457630902921287.
[50] E.S. Cho, J.W. Choi, J.S. Yoon, M.S. Kim, Modeling and simulation on the mass flow distribution in microchannel heat sinks with non-uniform heat flux conditions, Int. J. Heat Mass Transf. 53 (2010) 1341–1348, https://doi.org/10.1016/j.ijheatmasstransfer.2009.12.025.
[51] M. Saeed, M.-H. Kim, Header design approaches for mini-channel heatsinks using analytical and numerical methods, Appl. Therm. Eng. 110 (2017) 1500–1510, https://doi.org/10.1016/j.applthermaleng.2016.09.069.
[52] J.-Y. Song, S. Hah, D. Kim, S.-M. Kim, Enhanced flow uniformity in parallel mini-channels with pin-finned inlet header, Appl. Therm. Eng. 152 (2019) 718–733, https://doi.org/10.1016/j.applthermaleng.2019.02.069.
[53] J. Li, G.P. Peterson, P. Cheng, Three-dimensional analysis of heat transfer in a micro-heat sink with single phase flow, Int. J. Heat Mass Transf. 47 (2004) 4215–4231, https://doi.org/10.1016/j.ijheatmasstransfer.2004.04.018.
[54] W. Qu, I. Mudawar, Analysis of three-dimensional heat transfer in micro-channel heat sinks, Int. J. Heat Mass Transf. 45 (2002) 3973–3985, https://doi.org/10.1016/S0017-9310(02)00101-1.
[55] R.V. Rao, K.C. More, J. Taler, P. Ocłoń, Dimensional optimization of a micro-channel heat sink using Jaya algorithm, Appl. Therm. Eng. 103 (2016) 572–582, https://doi.org/10.1016/j.applthermaleng.2016.04.135.
[56] K. Vafai, L. Zhu, Analysis of two-layered micro-channel heat sink concept in electronic cooling, Int. J. Heat Mass Transf. 42 (1999) 2287–2297, https://doi.org/10.1016/S0017-9310(98)00017-9.
[57] K.-T. Chiang, C.-C. Chou, N.-M. Liu, Application of response surface methodology in describing the thermal performances of a pin-fin heat sink, Int. J. Therm. Sci. 48 (2009) 1196–1205, https://doi.org/10.1016/j.ijthermalsci.2008.10.009.
[58] K.-T. Chiang, Modeling and optimization of designing parameters for a parallel-plain fin heat sink with confined impinging jet using the response surface methodology, Appl. Therm. Eng. 27 (2007) 2473–2482, https://doi.org/10.1016/j.applthermaleng.2007.02.004.
[59] C.-C. Chou, N.-M. Liu, J.-T. Horng, K.-T. Chiang, Designing parameter optimization of a Parallel-Plain Fin heat sink using the grey-based fuzzy algorithm with the orthogonal arrays, Int. J. Therm. Sci. 48 (2009) 2271–2279, https://doi.org/10.1016/j.ijthermalsci.2009.04.012.
[60] A. Subasi, B. Sahin, I. Kaymaz, Multi-objective optimization of a honeycomb heat sink using Response Surface Method, Int. J. Heat Mass Transf. 101 (2016) 295–302, https://doi.org/10.1016/j.ijheatmasstransfer.2016.05.012.
[61] J. Wen, H. Yang, X. Tong, K. Li, S. Wang, Y. Li, Optimization investigation on configuration parameters of serrated fin in plate-fin heat exchanger using genetic algorithm, Int. J. Therm. Sci. 101 (2016) 116–125, https://doi.org/10.1016/j.ijthermalsci.2015.10.024.
[62] S. Kanyakam, S. Bureerat, Multiobjective optimization of a pin-fin heat sink using evolutionary algorithms, J. Electron. Packag. 134 (2012), https://doi.org/10.1115/1.4006514, 021008-021008–8.
[63] Y. Hadad, B. Ramakrishnan, R. Pejman, S. Rangarajan, P.R. Chiarot, A. Pattamatta, B. Sammakia, Three-objective shape optimization and parametric study of a micro-channel heat sink with discrete non-uniform heat flux boundary conditions, Appl. Therm. Eng. 150 (2019) 720–737, https://doi.org/10.1016/j.applthermaleng.2018.12.128.
[64] H.E. Ahmed, B.H. Salman, A.Sh Kherbeet, M.I. Ahmed, Optimization of thermal design of heat sinks: a review, Int. J. Heat Mass Transf. 118 (2018) 129–153, https://doi.org/10.1016/j.ijheatmasstransfer.2017.10.099.
[65] N.H. Naqiuddin, L.H. Saw, M.C. Yew, F. Yusof, T.C. Ng, M.K. Yew, Overview of micro-channel design for high heat flux application, Renew. Sustain. Energy Rev. 82 (2018) 901–914, https://doi.org/10.1016/j.rser.2017.09.110.
[66] B. Ramakrishnan, Y. Hadad, S. Alkharabsheh, P.R. Chiarot, B. Sammakia, Thermal analysis of cold plate for direct liquid cooling of high performance servers, J. Electron. Packag. 141 (2019), https://doi.org/10.1115/1.4044130, 041005-041005–10.
[67] V. Semin, M. Bardsley, O. Rosten, C. Aldham, Application of a multilevel unstructured staggered solver to thermal electronic simulations, in: 2015 31st Thermal Measurement, Modeling Management Symposium, SEMI-THERM), 2015, pp. 287–292, https://doi.org/10.1109/SEMI-THERM.2015.7100174.
[68] Y. Hadad, B. Ramakrishnan, S. Alkharabsheh, P.R. Chiarot, B. Sammakia, Numerical Modeling and Optimization of a V-Groove Warm Water Cold-Plate, Thermal Measurement, Modeling & Management Symposium (SEMI-THERM), 2017, https://doi.org/10.1109/SEMI-THERM.2017.7896948, 2017 33rd.
[69] R.K. Shah, A.L. London, Laminar Flow Forced Convection in Ducts, Academic Press, 1978.
[70] Y.S. Muzychka, M.M. Yovanovich, Laminar forced convection heat transfer in the combined entry region of non-circular ducts, J. Heat Transf. 126 (2004) 54–61, https://doi.org/10.1115/1.1643752.
[71] Y.S. Muzychka, M.M. Yovanovich, Pressure drop in laminar developing flow in noncircular ducts: a scaling and modeling approach, J. Fluids Eng. 131 (2009) 111105, https://doi.org/10.1115/1.4000377.

[72] D.R.S. Raghuraman, R. Thundil Karuppa Raj, P.K. Nagarajan, B.V.A. Rao, Influence of aspect ratio on the thermal performance of rectangular shaped micro channel heat sink using CFD code, Alexandria Eng. J. 56 (2017) 43–54, https://doi.org/10.1016/j.aej.2016.08.033.
[73] H.R. Upadhye, S.G. Kandlikar, Optimization of microchannel geometry for direct chip cooling using single phase heat transfer, in: American Society of Mechanical Engineers, 2004, pp. 679–685, https://doi.org/10.1115/ICMM2004-2398.
[74] W. Qu, I. Mudawar, Analysis of three-dimensional heat transfer in micro-channel heat sinks, Int. J. Heat Mass Transf. 45 (2002) 3973–3985, https://doi.org/10.1016/S0017-9310(02)00101-1.
[75] C. Hilbert, S. Sommerfeldt, O. Gupta, D.J. Herrell, High performance micro-channel air cooling, in: Sixth Annual IEEE Proceedings Semiconductor Thermal and Temperature Measurement Symposium, 1990, pp. 108–113, https://doi.org/10.1109/STHERM.1990.68500.
[76] Z. Duan, Y.S. Muzychka, Pressure drop of impingement air cooled plate fin heat sinks, J. Electron. Packag. 129 (2006) 190–194, https://doi.org/10.1115/1.2721094.
[77] S.B. Sathe, B.G. Sammakia, An analytical study of the optimized performance of an impingement heat sink, J. Electron. Packag. 126 (2005) 528–534, https://doi.org/10.1115/1.1827269.
[78] R. Venkata Rao, Jaya: A simple and new optimization algorithm for solving constrained and unconstrained optimization problems, Int. J. Indust. Eng. Comput. 7 (2016) 19–34.
[79] N. Zheng, P. Liu, Z. Liu, W. Liu, Numerical simulation and sensitivity analysis of heat transfer enhancement in a flat heat exchanger tube with discrete inclined ribs, Int. J. Heat Mass Transf. 112 (2017) 509–520, https://doi.org/10.1016/j.ijheatmasstransfer.2017.05.019.

Nomenclature

COP: Heat sink coefficient of performance
c_p: Specific heat capacity ($J/kg.K$)
k: Conductivity ($W/m.\ K$)
N: Number of channels
P: Pressure (Pa)
Q: Coolant volumetric flow rate (m^3/s)
$\dot{q}$: Chip power (W)
R_H: Hydraulic resistance ($1/m.\ s$)
R_{Th}: Thermal Resistance (K/W) or ($K.\ m^2/W$)
Re: Reynolds number
T: Temperature (K)
V: Velocity (m/s)
$\dot{w}_P$: Pump power (W)Geek symbols
μ: Absolute viscosity ($kg/m.\ s$)
ρ: Density (kg/m^3)Subscripts
Ch: Channel
Co: Collector
Di: Distributor
F: Fin
f: Fluid
In: Inlet
s: SolidSuperscripts
M: Maximum